Structural Engineering and Mechanics, *Vol. 56, No. 1 (2015) 137-156*
DOI: http://dx.doi.org/10.12989/sem.2015.56.1.137

Magneto-thermo-elastic response of a rotating functionally graded cylinder

Mohammad Hosseini* and Ali Dini

Department of Mechanical Engineering, Sirjan University of Technology, 78137-33385 Sirjan, I.R. Iran

(Received May 7, 2015, Revised October 4, 2015, Accepted October 5, 2015)

Abstract. In this paper, an analytical solution of displacement, strain and stress field for rotating thick-walled cylinder made of functionally graded material subjected to the uniform external magnetic field and thermal field in plane strain state has been studied. Stress, strain and displacement field as a function of radial coordinates considering magneto-thermo-elasticity are derived analytically. According to the Maxwell electro-dynamic equations, Lorentz force in term of displacement is obtained in cylindrical coordinates. Also, symmetric temperature distribution along the thickness of hollow cylinder is obtained by solving Fourier heat transfer equation in cylindrical coordinates. Using equation of equilibrium and thermo-mechanical constitutive equations associated with Lorentz force, a second-order inhomogeneous differential equation in term of displacement is obtained and will be solved analytically. Except Poisson's ratio, other mechanical properties such as elasticity modulus, density, magnetic permeability coefficient, heat conduction coefficient and thermal expansion coefficient are assumed to vary through the thickness according to a power law. In results analysis, non-homogeneity parameter has been chosen arbitrary and inner and outer surface of cylinder are assumed to be rich metal and rich ceramic, respectively. The effect of rotation, thermal, magnetic field and non-homogeneity parameter of functionally graded material which indicates percentages of cylinder's constituents are studied on displacement, Von Mises equivalent stress and Von Mises equivalent strain fields.

Keywords: analytical solution; functionally graded material; Magneto-thermo-elasticity; rotating thick-walled cylinder

1. Introduction

Thick-walled vessels are of significant equipment, especially used in oil, chemical, petroleum, petrochemical and nuclear branches and in most industries such as the power generation industry for fossil and nuclear power, the petrochemical industry for storing and processing crude petroleum oil in tank farms as well as storing gasoline in service stations, and the chemical industry for chemical reactors (Chattopadhyay 2004). Hence, focusing on their designing and building is important. In many cases, these vessels are simultaneously exposed to thermal and magnetic fields, which have significant effects on displacement, strain, and stress fields and thus on their performance.

*Corresponding author, Ph.D., E-mail: hosseini@sirjantech.ac.ir

http://www.techno-press.org/?journal=sem&subpage=8 ISSN: 1225-4568 (Print), 1598-6217 (Online)

To improve the performance of these vessels with regard to their operating conditions, functionally graded materials (FGMs) can be utilized. These materials are widely applied in many fields such as aerospace and nuclear engineering. Functionally graded materials are advanced materials with high thermal resistance, which are employed as intelligent structures in modern technology. In addition to good thermal properties, they have significant resistance to fracture and corrosion. In contrast to traditional construction materials FGM are heterogeneous and their mechanical properties, such as elasticity modulus, density, thermal conductivity coefficient, etc., change gradually with position.

A common type of such materials includes ceramic and metal phases, in which their changes from one surface to another occur quite continuously. This is due to gradually combination of pure ceramic and metal between the two surfaces.

Operation of vessels under different thermal conditions and magnetic fields leads to a disparate distribution of displacement, strain, and stress fields in comparison with a situation where the mentioned conditions do not exist. So far, several studies on the magneto-elastic and magneto-thermo-elastic behaviors of pressure vessels made of FGMs have been conducted, some of which are noted as follows.

Thermo-mechanical analysis of cylinders and plates made of FGMs has been done by Reddy and Chin (1998). They solved thermo-elastic and heat transfer equations for axisymmetric cylinders under thermal loading using finite element model. Eslami *et al*. (2005) provided a general one-dimensional solution to steady mechanical and thermal stresses in a thick-walled sphere made of FGMs. Given the assumption that the mechanical and thermal properties are based on variable power-law in the thickness direction of the sphere, they analytically solved heat transfer and Navier equations. Peng and Li (2010) studied thermo-elastic analysis of cylinders made of FGMs. They assumed varying material properties in the radial direction of the cylinder and obtained thermal stress distribution and radial displacement through the numerical solution of the equations. Furthermore, they examined the effects of the material non-homogeneity parameter on thermal stress. Dai *et al*. (2006) offered the exact solution of cylindrical and spherical pressure vessels made of FGMs with power law distribution within a uniform magnetic field. They assumed FGM properties vary in the radial direction according to power law distribution and thus accurately solved the acquired equations. Moreover, they investigated the effects of material non-homogeneity parameter on the stress distribution and perturbation of magnetic fields. Tutuncu and Ozturk (2001) introduced an analytical solution for displacements and stresses in spherical and cylindrical vessels under internal pressure. They considered the properties as a power-law and addressed arbitrary non-homogeneity parameter effects on stress distribution. Naghdabadi and Hosseini Kordkheili (2005) extracted the relations of finite element for the analysis of thermo-elastic shells and plates made of FGMs. They used Rayleigh-Ritz method for solving nonlinear equations of heat transfer. Ruhi *et al*. (2005) offered an analytical thermo-elastic solution for long thick-walled cylinders made of FGMs. Using Fourier series expansion, they transformed partial differential equations into ordinary differential equations. Also, by taking into account the effects of thermal loading and uniformly internal pressure, they showed non-homogeneity parameter is the most efficient parameter in the thermo-mechanical response of a cylinder made of FGMs. Lutz and Zimmerman (1996) provided a precise solution for the thermal stresses of spheres made of FGMs, in which Young's modulus and thermal expansion coefficient vary linearly with radius. Obata and Noda (1994) examined thermal stresses in hollow cylinders and hollow spheres made of a functionally gradient material. The aim of their research was to understand the effect of the composition on stresses and to design the optimum FGM hollow circular cylinder and hollow

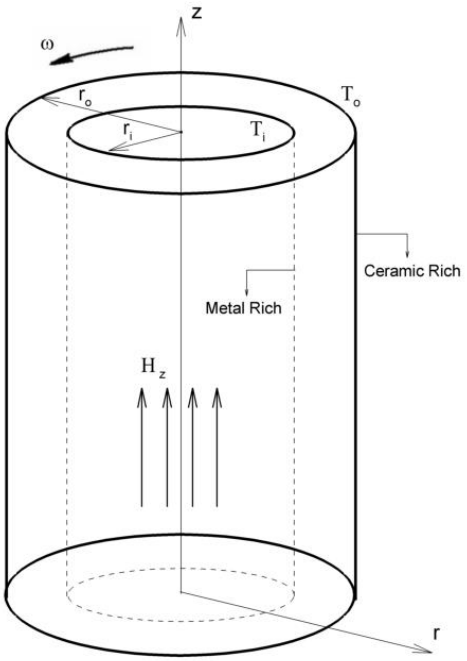

Fig. 1 A hollow rotating cylinder in magnetic and thermal fields

sphere. Tokovyy and Ma (2007) investigated the two-dimensional asymmetric elasticity and thermo-elasticity problems for non-homogeneous hollow cylinders. They used direct integration method to solve the governing equations in the form of Fourier series. Also, an elastic analysis for axisymmetric clamped-clamped pressurized thick truncated conical shells made of functionally graded materials using first-order shear deformation theory (FSDT) and the virtual work principle performed by Ghannad *et al*. (2012). In another work, Ghannad and Gharooni (2014) presented an analytical formulation based on the FSDT for thick-walled cylinders made of functionally graded materials under internal and external uniform pressure. Recently, the electro-magneto-thermo-elastic behavior of a rotating functionally graded long hollow cylinder with functionally graded piezoelectric layers was analytically analyzed by Saadatfar and Aghaie-Khafri (2015).

According to the studies conducted, no research has been already performed on the analytical solutions of displacement, stress, and strain for a rotating hollow cylinder made of FGMs in a plane strain state based on magneto-thermo-elasticity theory. Therefore, this study was targeted at this issue. Displacement, stress, and strain fields were extracted as a radial function derived by analytical solution. The mechanical properties of FGMs were assumed to be variable as power law of radius to derive displacement, stress, and strain equations. Thermal distribution in a long hollow cylinder was achieved by solving the heat transfer equation in the steady state. Thus, despite the magnetic and thermal fields, equilibrium equations were extracted for a rotating cylinder made from FGMs. By inserting the stress equations into a mechanical equilibrium equation, a differential equation of order two was obtained in terms of displacement. Finally, through the analytical solution of the resulting equation, the effects of non-homogeneity parameter of FGMs, magnetic field, and temperature change on the displacement, strain, and stress fields were illustrated in this article.

2. Description of the problem and governing equations

A hollow cylinder made of FGMs (metallic-ceramic) was considered with the inner and outer radii of r_i and r_o, respectively, in a uniform magnetic field of $\vec{H} = (0,0,H_z)$ and a constant angular velocity of ω. H_z is the component of magnetic field in the direction of Z axis. Also, temperatures of the inner and outer surfaces were regarded as T_i and T_o, respectively (Fig. 1).

Poisson's ratio is considered to be constant but other properties such as elasticity modulus, coefficient of magnetic permeability, density, thermal conductivity coefficient, and thermal expansion coefficient change according to relations $E(\bar{r}) = E_0\bar{r}^{\beta}$, $\mu(\bar{r}) = \mu_0\bar{r}^{\beta}$, $\rho(\bar{r}) = \rho_0\bar{r}^{\beta}$, $k(\bar{r}) = k_0\bar{r}^{\beta}$, and $\alpha(\bar{r}) = \alpha_0\bar{r}^{\beta}$, respectively. Here, E_0, μ_0, ρ_0, k_0, and α_0 are the corresponding elastic properties of the outer surface ($r = r_o$) and β is the non-homogeneity parameter of the FGMs, representing the volume fraction percentage of its components. Also, $\bar{r} = \frac{r}{r_o}$ is the variable of dimensionless radius and r is the radius of an arbitrary point on the cylinder.

By applying a magnetic field, consequently a magnetic vector distributing $\vec{h}$, a strength vector of the electric field $\vec{e}$, and a Lorentz force vector f_r were created in the FGMs. Assuming that the magnetic permeability of the outer surface of the rotating cylinder is equal to the magnetic permeability of its surrounding environment, the governing equations of Maxwell electrodynamics for a conductive elastic body can be written as follows (Dai and Wang 2004, Karus 1984)

$$\vec{J} = \vec{\nabla} \times \vec{h} \tag{1a}$$

$$\vec{\nabla} \cdot \vec{h} = 0 \tag{1b}$$

$$\vec{e} = -\mu(\bar{r})\left(\frac{\partial \vec{u}}{\partial t} \times \vec{H}\right) \tag{1c}$$

$$\vec{h} = \vec{\nabla} \times \left(\vec{U} \times \vec{H}\right) \tag{1d}$$

$$\vec{\nabla} \times \vec{e} = -\mu(\bar{r})\frac{\partial \vec{h}}{\partial t} \tag{1e}$$

In the above equations, vector $\vec{J}$ is the electric current density. By employing a magnetic field vector of $\vec{H}$ in the cylindrical coordinates of (r,θ,z) in Eq. (1), the following relations are obtained

$$\vec{U} = (u,0,0) \tag{2a}$$

$$\vec{h} = (0,0,h_z) \tag{2b}$$

$$h_z = -H_z\left(\frac{\partial u}{\partial r} + \frac{u}{r}\right) \tag{2c}$$

$$\vec{J} = \left(0, -\frac{\partial h_z}{\partial r}, 0\right) \tag{2d}$$

$$\vec{e} = -\mu(\bar{r})\left(0, H_z \frac{\partial u}{\partial t}, 0\right) \tag{2e}$$

Where u is the displacement of an arbitrary point in the radial direction. Under the effect of the magnetic field, Lorentz magnetic force vector is calculated from the following equation

$$[f_r, f_\theta, f_z] = \mu(\bar{r})\left(\vec{J} \times \vec{H}\right) = \left[\mu_0 H_z^2 \frac{\partial}{\partial r}\left(\bar{r}^\beta \frac{\partial u}{\partial r} + \bar{r}^\beta \frac{u}{r}\right), 0{,}0\right] \tag{3}$$

Where f_r, f_θ, and f_z are Lorentz force components in the directions of radial, tangential, and axial coordinates, respectively.

Dynamic electromagnetics equations for the rotating cylinders made of FGMs with considering the Lorentz force can be expressed as follows

$$\frac{\partial \sigma_r}{\partial r} + \frac{\sigma_r - \sigma_\theta}{r} + f_r + \rho\omega^2 r = 0 \tag{4}$$

Where σ_r, σ_θ, and ρ are radial and circumferential stresses and densities at an arbitrary point, respectively.

2.1 Magneto-elastic solution

For a magneto-elastic solution, it is assumed that there is no thermal load, i.e., $T_i = T_o = 0$. In the case of plane strain, radial and circumferential stresses for a long hollow cylinder are expressed as follows (Dai *et al*. 2006)

$$\sigma_r = \frac{E(\bar{r})}{(1+\vartheta)(1-2\vartheta)}\left[(1-\vartheta)\frac{\partial u}{\partial r} + \vartheta \frac{u}{r}\right] \tag{5a}$$

$$\sigma_\theta = \frac{E(\bar{r})}{(1+\vartheta)(1-2\vartheta)}\left[\vartheta \frac{\partial u}{\partial r} + (1-\vartheta)\frac{u}{r}\right] \tag{5b}$$

By substituting Eq. (3) and Eq. (5) into Eq. (4), the dimensionless Cauchy-Euler equation with non-homogenous part is obtained based on the relations $\bar{r} = \frac{r}{r_o}$ and $\bar{u} = \frac{u}{r_o}$

$$\bar{r}^2 \frac{\partial^2 \bar{u}}{\partial \bar{r}^2} + (\beta+1)\bar{r}\frac{\partial \bar{u}}{\partial \bar{r}} + (\lambda\beta - 1)\bar{u} + \delta\bar{r}^3 = 0 \tag{6a}$$

$$\lambda = \frac{E_0\vartheta + \mu_0 H_z^2(1+\vartheta)(1-2\vartheta)}{E_0(1-\vartheta) + \mu_0 H_z^2(1+\vartheta)(1-2\vartheta)} \tag{6b}$$

$$\delta = \frac{\rho_0\omega^2 r_o^2(1+\vartheta)(1-2\vartheta)}{E_0(1-\vartheta) + \mu_0 H_z^2(1+\vartheta)(1-2\vartheta)} \tag{6c}$$

The characteristic equation for solving the homogeneous part of Cauchy-Euler equation and its roots is as the following

$$m^2 + \beta m + (\lambda\beta - 1) = 0 \tag{7a}$$

$$m_1 = \frac{1}{2}\left(-\beta - \sqrt{\beta^2 - 4\lambda\beta + 4}\right) \tag{7b}$$

$$m_2 = \frac{1}{2}\left(-\beta + \sqrt{\beta^2 - 4\lambda\beta + 4}\right) \tag{7c}$$

Therefore, a general solution to Eq. (6a) appears as follows

$$\bar{u}_h(\bar{r}) = C_1\bar{r}^{m_1} + C_2\bar{r}^{m_2} \tag{8}$$

and the particular solution to Eq. (6a) is obtained as the following

$$\bar{u}_p(\bar{r}) = \frac{-\delta}{\beta(3+\lambda)+8}\bar{r}^3 \tag{9}$$

Thus, the general solution of Eq. (6a) can be expressed for plane strain state according to Eqs. (8) and (9) as follows

$$\bar{u}_t(\bar{r}) = C_1\bar{r}^{m_1} + C_2\bar{r}^{m_2}\bar{u}_p(\bar{r}) - \frac{\delta}{\beta(3+\lambda)+8}\bar{r}^3 \tag{10}$$

By inserting Eq. (10) in Eq. (5), the relations of radial and circumferential stresses are defined as the following

$$\sigma_r = \frac{E_0}{(1+\vartheta)(1-2\vartheta)}\left\{[(1-\vartheta)m_1+\vartheta]C_1\bar{r}^{m_1+\beta-1} + [(1-\vartheta)m_2+\vartheta]C_2\bar{r}^{m_2+\beta-1} - \frac{(3-2\vartheta)\delta}{\beta(3+\lambda)+8}\bar{r}^{\beta+2}\right\} \tag{11a}$$

$$\sigma_\theta = \frac{E_0}{(1+\vartheta)(1-2\vartheta)}\left\{[(1-\vartheta)+m_1\vartheta]C_1\bar{r}^{m_1+\beta-1} + [(1-\vartheta)+m_2\vartheta]C_2\bar{r}^{m_2+\beta-1} - \frac{(1+2\vartheta)\delta}{\beta(3+\lambda)+8}\bar{r}^{\beta+2}\right\} \tag{11b}$$

According to Eq. (10), strains are as follows

$$\varepsilon_r = \frac{\partial\bar{u}}{\partial\bar{r}} = m_1C_1\bar{r}^{m_1-1} + m_2C_2\bar{r}^{m_2-1} - \frac{3\delta}{\beta(3+\lambda)+8}\bar{r}^2 \tag{12a}$$

$$\varepsilon_\theta = \frac{\bar{u}}{\bar{r}} = C_1\bar{r}^{m_1-1} + C_2\bar{r}^{m_2-1} - \frac{\delta}{\beta(3+\lambda)+8}\bar{r}^2 \tag{12b}$$

Also, C_1 and C_2 constants are calculated by boundary conditions (13)

$$\sigma_r\left(\bar{r} = \frac{r_i}{r_o}\right) = 0 \tag{13a}$$

$$\sigma_r\left(\bar{r} = \frac{r_o}{r_o} = 1\right) = 0 \tag{13b}$$

2.2 Magneto-thermo-elastic solution

To obtain stress under thermal field effect in a hollow cylinder made of FGMs, it is necessary to first obtain the temperature distributions in cylinders. Here, we assumed the cylinder is in the steady state without internal heat generation. Fourier heat transfer equation in cylindrical coordinates can be expressed as the following

$$\frac{1}{r}\frac{d}{dr}\left(rk(r)\frac{dT(r)}{dr}\right)=0 \tag{14}$$

Where $T(r)$ is the temperature change in terms of radius. Thermal boundary conditions for the cylinder are as follows

$$T(r=r_i)=T_i \tag{15a}$$

$$T(r=r_o)=T_o \tag{15b}$$

By simplifying Eq. (14), Cauchy Euler differential equation for temperature will be achieved as the following

$$r^2\frac{d^2T(r)}{d^2r}+(\beta+1)r\frac{dT(r)}{dr}=0 \tag{16}$$

Thus, by solving Eq. (16), temperature distribution in the hollow cylinder can be expressed as follows

$$T(\bar{r})=A+B\bar{r}^{(-\beta)} \tag{17}$$

Where A and B are constants, which determined by thermal boundary conditions (15) as

$$A=T_i+\frac{r_o^{\beta}(T_i-T_o)}{r_i^{\beta}-r_o^{\beta}} \tag{18a}$$

$$B=-\frac{r_i^{\beta}(T_i-T_o)}{r_i^{\beta}-r_o^{\beta}} \tag{18b}$$

At the presence of thermal field, radial and circumferential stresses of σ_r^T and σ_θ^T for hollow cylinders are expressed as the following

$$\sigma_r^T=\frac{E(\bar{r})}{(1+\vartheta)(1-2\vartheta)}\left[(1-\vartheta)\frac{\partial u}{\partial r}+\vartheta\frac{u}{r}\right]-\frac{E(\bar{r})\alpha(\bar{r})}{(1-2\vartheta)}\Delta T(\bar{r}) \tag{19a}$$

$$\sigma_\theta^T=\frac{E(\bar{r})}{(1+\vartheta)(1-2\vartheta)}\left[\vartheta\frac{\partial u}{\partial r}+(1-\vartheta)\frac{u}{r}\right]-\frac{E(\bar{r})\alpha(\bar{r})}{(1-2\vartheta)}\Delta T(\bar{r}) \tag{19b}$$

Where $\Delta T(\bar{r})=T(\bar{r})-T^*$ and T^* are reference temperatures considered to be 25℃. By substituting Eqs. (3), (17), and (19) in Eq. (4), Cauchy-Euler equation with its non-homogeneous part is achieved. Then, by making it dimensionless based on relations $\bar{r}=\frac{r}{r_o}$ and $\bar{u}=\frac{u}{r_o}$, the following equation will be resulted

$$\bar{r}^2\frac{\partial^2\bar{u}}{\partial\bar{r}^2}+(\beta+1)\bar{r}\frac{\partial\bar{u}}{\partial\bar{r}}+(\lambda\beta-1)\bar{u}+\delta\bar{r}^3-\nabla\bar{r}^{\beta+1}-\Gamma\bar{r}=0 \tag{20a}$$

$$\lambda=\frac{E_0\vartheta+\mu_0H_z^2(1+\vartheta)(1-2\vartheta)}{E_0(1-\vartheta)+\mu_0H_z^2(1+\vartheta)(1-2\vartheta)} \tag{20b}$$

$$\delta=\frac{\rho_0\omega^2r_o^2(1+\vartheta)(1-2\vartheta)}{E_0(1-\vartheta)+\mu_0H_z^2(1+\vartheta)(1-2\vartheta)} \tag{20c}$$

$$\nabla=\frac{2E_0\alpha_0\beta(1+\vartheta)A}{E_0(1-\vartheta)+\mu_0H_z^2(1+\vartheta)(1-2\vartheta)} \tag{20d}$$

$$\Gamma=\frac{E_0\alpha_0\beta(1+\vartheta)B}{[E_0(1-\vartheta)+\mu_0H_z^2(1+\vartheta)(1-2\vartheta)]} \tag{20d}$$

To solve the homogeneous part of Cauchy-Euler equation, Eq. (7) was used. The general solution to Eq. (20a) is equal to

$$\bar{u}_h(\bar{r})=C_3\bar{r}^{m_1}+C_4\bar{r}^{m_2} \tag{21}$$

Also, the particular solution to Eq. (20a) is obtained as follows

$$\bar{u}_p(\bar{r})=-\frac{\delta}{\beta(3+\lambda)+8}\bar{r}^3+\frac{\nabla}{\beta(2\beta+\lambda+3)}\bar{r}^{\beta+1}+\frac{\Gamma}{\beta(\lambda+1)}\bar{r} \tag{22}$$

Thus, the general solution of Eq. (20a) in the plane strain state can be expressed according to Eqs. (21) and (22) as the following

$$\bar{u}_t^T(\bar{r})=C_3\bar{r}^{m_1}+C_4\bar{r}^{m_2}-\frac{\delta}{\beta(3+\lambda)+8}\bar{r}^3+\frac{\nabla}{\beta(2\beta+\lambda+3)}\bar{r}^{\beta+1}+\frac{\Gamma}{\beta(\lambda+1)}\bar{r} \tag{23}$$

By inserting Eq. (23) into Eq. (19), stress equations in the presence of thermal field are defined as follows

$$\begin{aligned}\sigma_r^T=&\frac{E_0}{(1+\vartheta)(1-2\vartheta)}\{[(1-\vartheta)m_1+\vartheta]C_3\,\bar{r}^{m_1+\beta-1}+[(1-\vartheta)m_2+\vartheta]C_4\bar{r}^{m_2+\beta-1}-\\&\frac{(3-2\vartheta)\delta}{\beta(3+\lambda)+8}\bar{r}^{\beta+2}+\frac{(1+\beta(1-\vartheta))\nabla}{\beta(2\beta+\lambda+3)}\bar{r}^{2\beta}+\frac{\Gamma}{\beta(\lambda+1)}\bar{r}^{\beta}\Big\}-\frac{E_0\alpha_0}{(1-2\vartheta)}\left(A\bar{r}^{2\beta}+B\bar{r}^{\beta}\right)\end{aligned} \tag{24a}$$

$$\begin{aligned}\sigma_\theta^T=&\frac{E_0}{(1+\vartheta)(1-2\vartheta)}\{[(1-\vartheta)+m_1\vartheta]C_3\bar{r}^{m_1+\beta-1}+[(1-\vartheta)+m_2\vartheta]C_4\bar{r}^{m_2+\beta-1}-\\&\frac{(1+2\vartheta)\delta}{\beta(3+\lambda)+8}\bar{r}^{\beta+2}+\frac{(1+\beta\vartheta)\nabla}{\beta(2\beta+\lambda+3)}\bar{r}^{2\beta}+\frac{\Gamma}{\beta(\lambda+1)}\bar{r}^{\beta}\Big\}-\frac{E_0\alpha_0}{(1-2\vartheta)}\left(A\bar{r}^{2\beta}+B\bar{r}^{\beta}\right)\end{aligned} \tag{24b}$$

And strains are defined as the following

$$\begin{aligned}\varepsilon_r^T=\frac{\partial\bar{u}}{\partial\bar{r}}=&m_1C_3\bar{r}^{m_1-1}+m_2C_4\bar{r}^{m_2-1}+\frac{\Gamma}{\beta(\lambda+1)}-\frac{3\delta}{\beta(3+\lambda)+8}\bar{r}^2\\&+\frac{(1+\beta)\nabla}{\beta(2\beta+\lambda+3)}\bar{r}^{\beta}\end{aligned} \tag{25a}$$

$$\varepsilon_\theta^T = \frac{\bar{u}}{\bar{r}} = C_3\bar{r}^{m_1-1} + C_4\bar{r}^{m_2-1} - \frac{\delta}{\beta(3+\lambda)+8}\bar{r}^2 + \frac{\nabla}{\beta(2\beta+\lambda+3)}\bar{r}^\beta + \frac{\Gamma}{\beta(\lambda+1)} \tag{25b}$$

C_3 and C_4 constants are calculated by boundary conditions (13). In many cases, use of equivalent stresses obtained based on von Mises criterion would be suitable for designing. Therefore, equivalent stress and strain are expressed by the following relations

$$\sigma_e = \left(\sigma_r^2 + \sigma_\theta^2 - \sigma_r\sigma_\theta\right)^{1/2} \tag{26a}$$

$$\varepsilon_e = \left(\varepsilon_r^2 + \varepsilon_\theta^2 - \varepsilon_r\varepsilon_\theta\right)^{1/2} \tag{26b}$$

3. Discussion and numerical results

3.1 Validiation

To confirm the results achieved in this paper, the results were compared with those reported by Jabbari *et al*. (2002) in a certain state. In this mode, in the absence of a magnetic field and with a zero temperature of outer surface, the properties were considered as follows

$E_0 = E_{cer} = 200\ (GPa)$, $\rho_0 = \rho_{cer} = 5700\ (^{kg}/_{m^3})$,

$P_i = 50\ (MPa)$, $T_i = 10\ (℃)$,

$\vartheta = 0.3$, $\alpha_0 = 1.2 \times 10^{-6}\ (^1/_{℃})$.

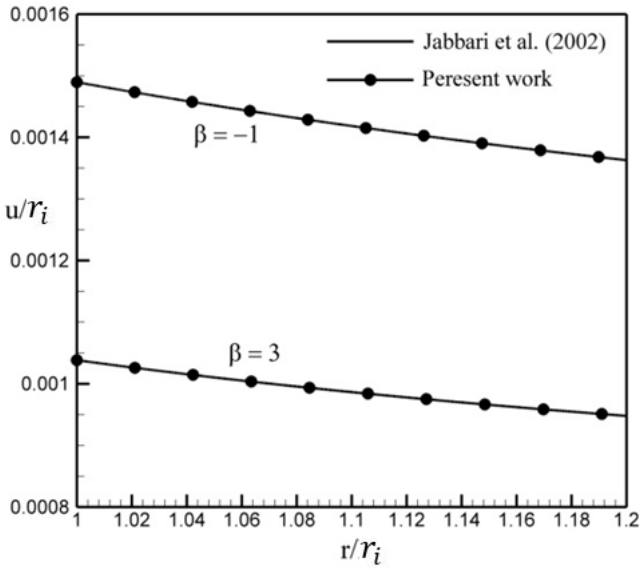

Fig. 2 Comparison between results of present work and Jabbari *et al*. (2002) for dimensionless radial displacement in the case of $H_z = 0$

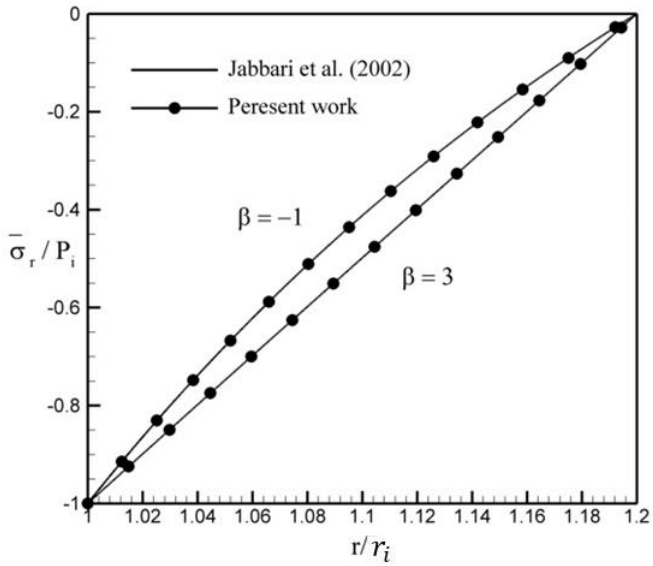

Fig. 3 Comparison between results of present work and Jabbari *et al.* (2002) for dimensionless radial stress in the case of $H_z = 0$

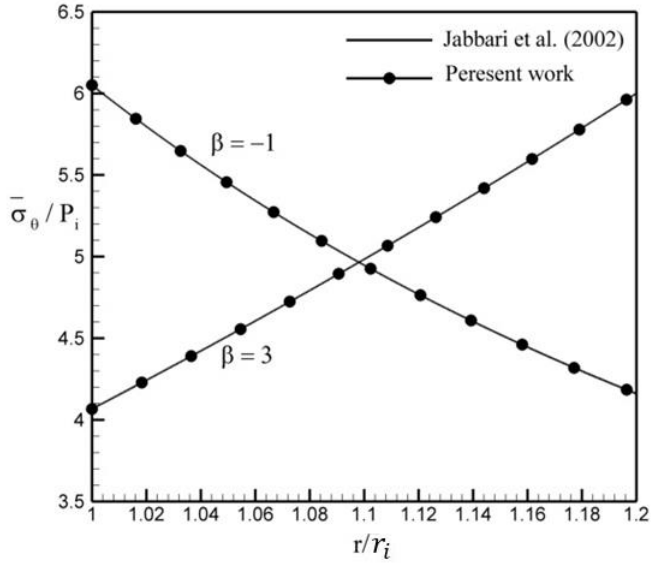

Fig. 4 Comparison between results of present work and Jabbari *et al.* (2002) for dimensionless circumferential stress in the case of $H_z = 0$

As it is obvious from Figs. 2-4, the results fulfill with Jabbari *et al*. (2002) very well. In the following, analysis of a cylinder made of a type of functionally graded (ceramic-metal) materials with the inner and outer radii of $r_i = 0.5\,m$ and $r_o = 1\,m$, respectively, will be addressed based on the following properties:

$E_0 = E_{cer} = 151(GPa)$, $\rho_0 = \rho_{cer} = 5700\ (^{kg}/_{m^3})$, $\mu_0 = 4\pi \times 10^{-7}\ (^{H}/_{m})$,

$\vartheta = 0.3$, $\alpha_0 = 1.2 \times 10^{-6}(^{1}/_{^oC})$, $\omega = 100\ (^{rad}/_{s})$.

3.2 Magneto-elastic analysis

For the analysis of a rotating cylinder, the outer surface was assumed to be pure ceramic. Also, to present the numerical results, it is convenient to use formal dimensionless and normalized displacement, stress, and strain as follows

$$\bar{u} = \frac{\bar{u}_t E_0}{\rho_0 \omega^2 r_o^3}, \bar{\sigma}_e = \frac{\sigma_e}{\rho_0 \omega^2 r_o^2}, \bar{\varepsilon}_e = \frac{\varepsilon_e E_0}{\rho_0 \omega^2 r_o^2} \tag{27}$$

Figs. 5-7 show the effects of non-homogeneity parameters on the displacement and equivalent stress and strain. According to Fig. 5, it can be seen that radial displacement increases with an increase in non-homogeneity parameter. This is due to this fact that an increase in the non-homogeneity parameter reduces the stiffness of the whole thick-walled cylinder. It was also observed that maximum and minimum displacements occur at the inner and outer surfaces of the cylinder, respectively. Fig. 6 displays that equivalent stress is reduced by a steady enhancement in non-homogeneity parameter. Within a radius of more than 0.85, the equivalent stress trend is reversed and increases with an increase in non-homogeneity parameter. Based on Fig. 7, the equivalent strain increases with an increment of non-homogeneity parameter. For every non-homogeneity parameter, a reduction of equivalent strain can be observed in terms of radius. In this figure, the maximum and minimum strains are shown to occur on the inner and outer surfaces of the cylinder, respectively.

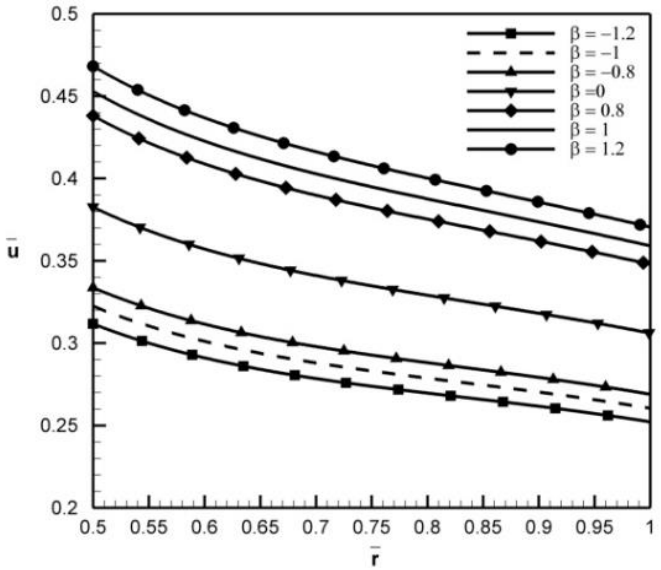

Fig. 5 The effects of non-homogeneity parameter β on the dimensionless radial displacement distribution, $H_z = 10^8 (^{A}/_{m})$

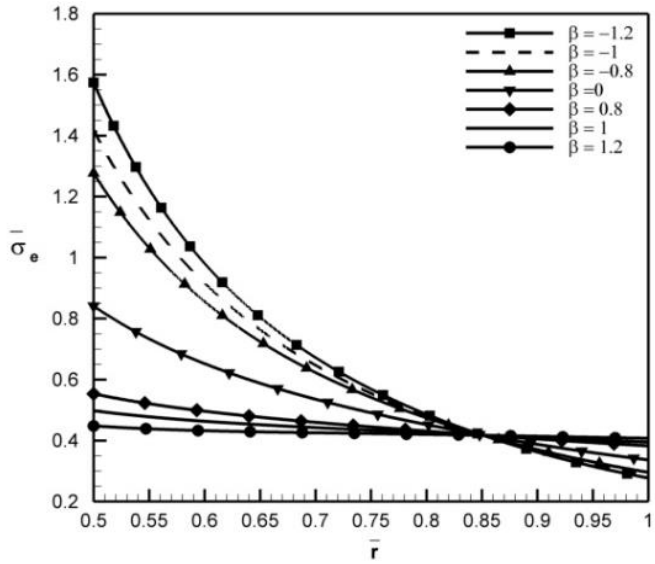

Fig. 6 The effects of non-homogeneity parameter β on the dimensionless equivalent stress distribution, $H_z = 10^8 (A/m)$

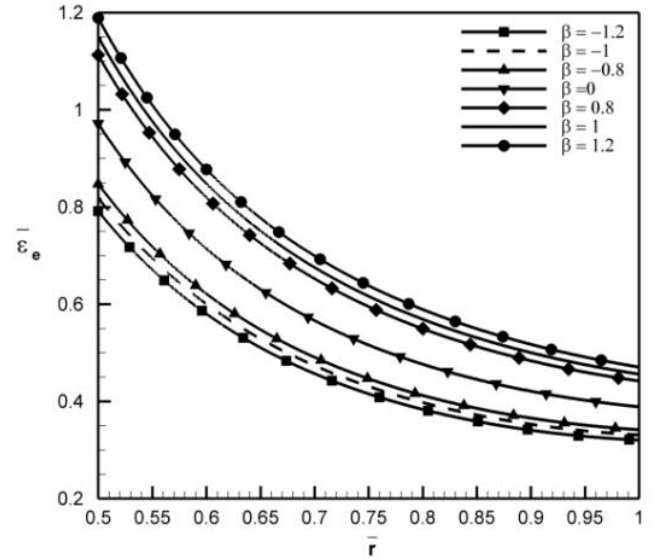

Fig. 7 The effects of non-homogeneity parameter β on the dimensionless equivalent strain distribution, $H_z = 10^8 (A/m)$

Figs. 8-10 demonstrate magnetic field effects on the displacement and equivalent stress and strain distributions caused by non-homogeneity effects. In Fig. 8, it is shown that radial displacement is reduced with increasing magnetic field. Additionally, it is perceived that based on each magnetic field, radial displacement displays a descending behavior depending on radius. Fig. 9 represents reduced values of equivalent stress with increasing magnetic field. Within each value of magnetic field, the equivalent stress decreases with increasing radius. Furthermore, it can be

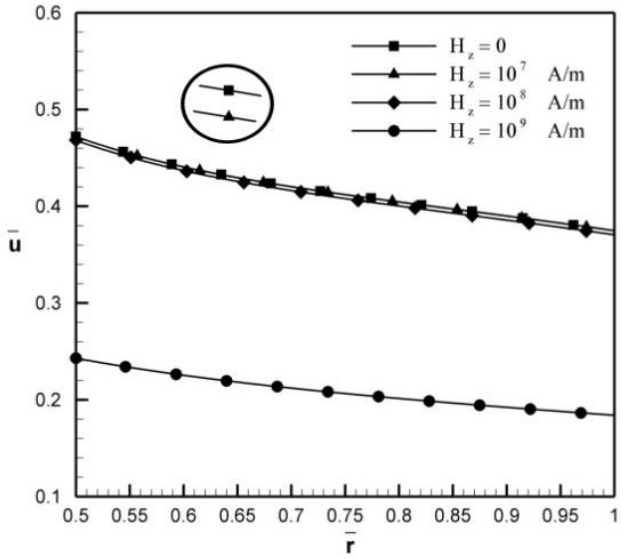

Fig. 8 The effects of magnetic field H_z on the dimensionless radial displacement distribution, $\beta = 1.2$

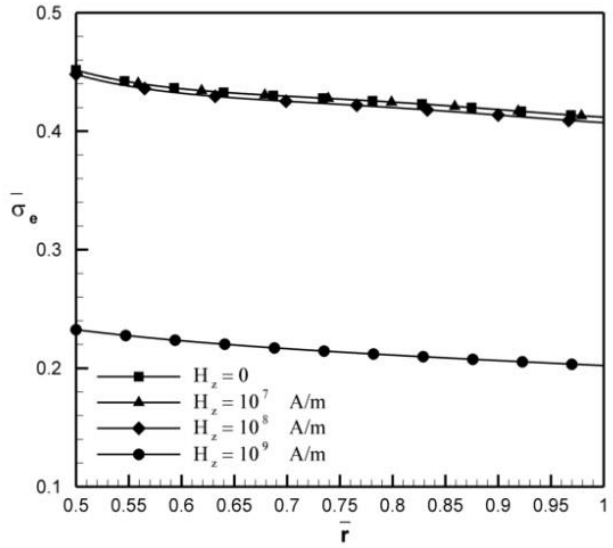

Fig. 9 The effects of magnetic field H_z on the dimensionless equivalent stress distribution, $\beta = 1.2$

found that maximum equivalent stress occurs at the inner surface.

In Fig. 10, it can be seen that increasing magnetic field is associated with decreased levels of the equivalent strain. According to Figs. 8-10, magnetic field values of $H_z > 10^7 (^A/_m)$ can be observed to have significant effects on the displacement and equivalent stress and strain.

3.3 Magneto-thermo-elastic analysis

In this section, the temperatures of the cylinder inner and outer surfaces were considered to be

$T_i = 25^{\circ}C$ and $T_o = 100^{\circ}C$, respectively. For simplicity, we define dimensionless displacement, stress, and strain as

$$\bar{u} = \frac{\bar{u}_t^T}{T_o \alpha_0 r_o}, \bar{\sigma}_e = \frac{\sigma_e}{T_o \alpha_0 E_0}, \bar{\varepsilon}_e = \frac{\varepsilon_e}{T_o \alpha_0} \tag{28}$$

Fig. 11 displays dimensionless temperature distribution in terms of dimensionless radius. According to this figure, it can be seen that temperature is enhanced by increasing non-homogeneity parameter. Moreover, temperature rises at each non-homogeneity parameter based on radius.

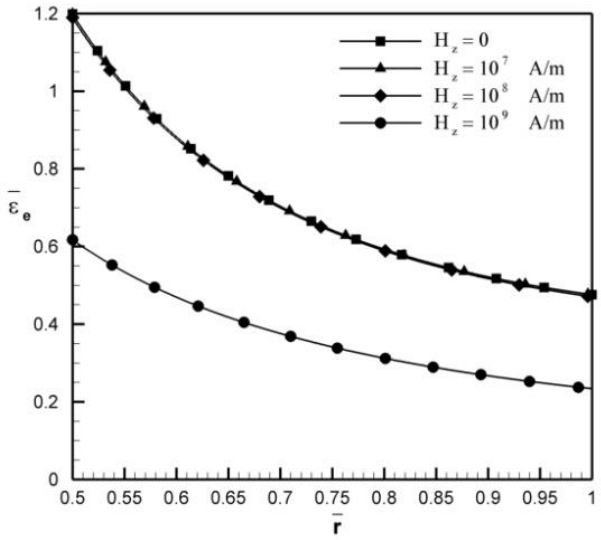

Fig. 10 The effects of magnetic field H_z on the dimensionless equivalent strain distribution, $\beta = 1.2$

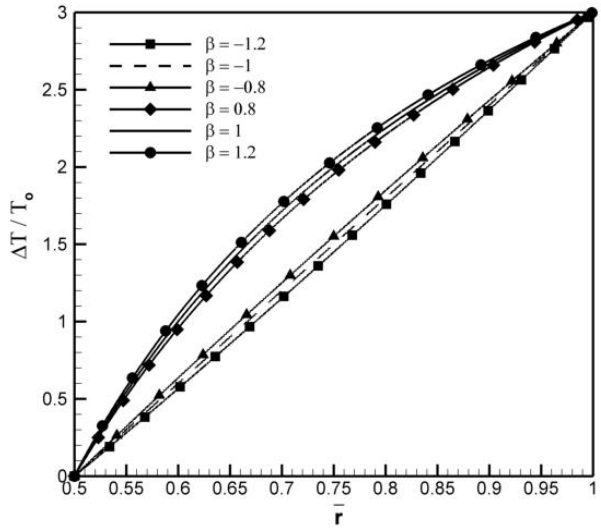

Fig. 11 Radial distribution of temperature in FGM rotating cylinder, ($T_i = 25^{\circ}C$, $T_o = 100^{\circ}C$)

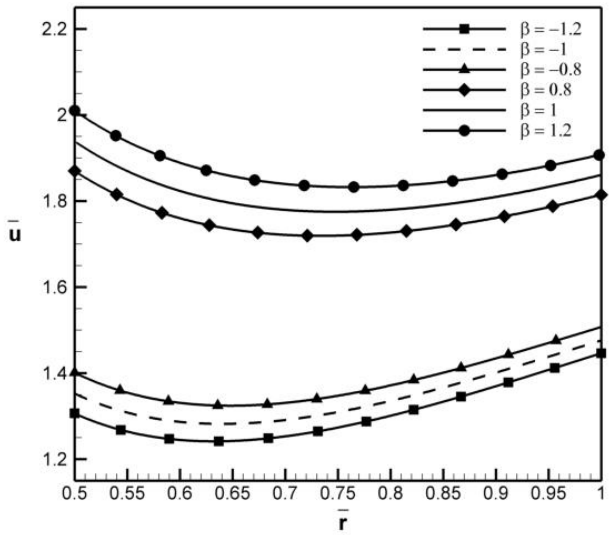

Fig. 12 The effects of non-homogeneity parameter β on the dimensionless radial displacement distribution, ($T_i = 25^{\circ}C$, $T_o = 100^{\circ}C$, $H_z = 10^8 (A/m)$)

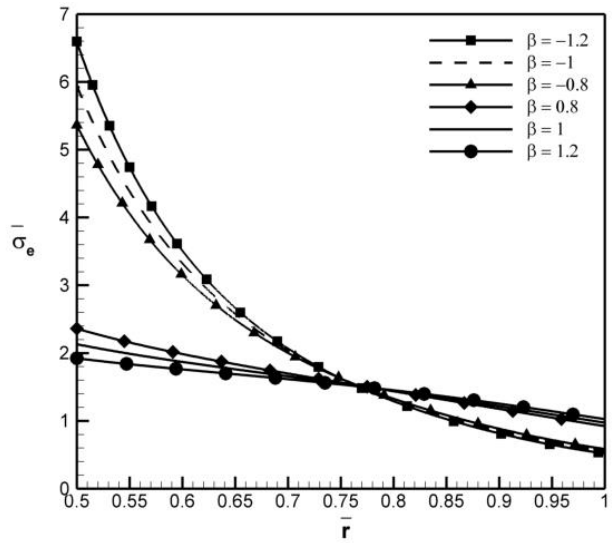

Fig. 13 The effects of non-homogeneity parameter β on the dimensionless equivalent stress distribution. ($T_i = 25^{\circ}C$, $T_o = 100^{\circ}C$, $H_z = 10^8 (A/m)$)

Figs. 12-14 represent the distributions of displacement and equivalent stress and strain in terms of the dimensionless radius at the presence of thermal and magnetic fields for various values of the non-homogeneity parameter. In Fig. 12, radial displacement enhancement with increasing non-homogeneity parameter can be observed. Radial displacement based on radius first decreases and then increases in terms of each value of non-homogeneity parameter.

In Fig. 13, it is shown that the equivalent stress is reduced with the increase of non-homogeneity parameter within a radius of less than 0.75; however, it increases with increasing

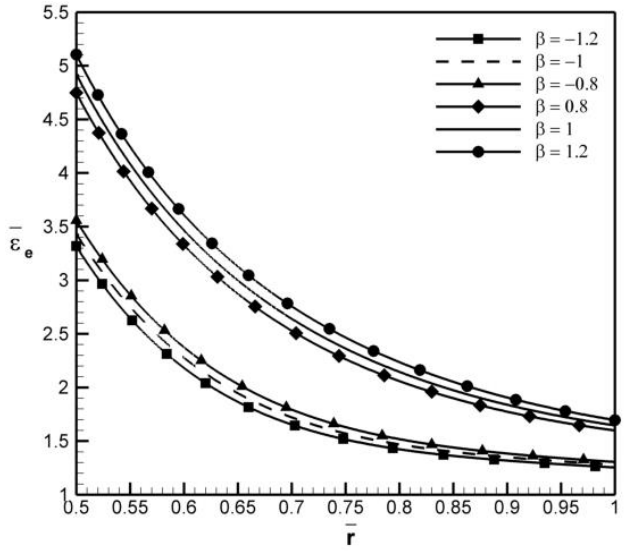

Fig. 14 The effects of non-homogeneity parameter β on the dimensionless equivalent strain distribution. ($T_i = 25^{\circ}C$, $T_o = 100^{\circ}C$, $H_z = 10^8 (^{A}/_{m})$)

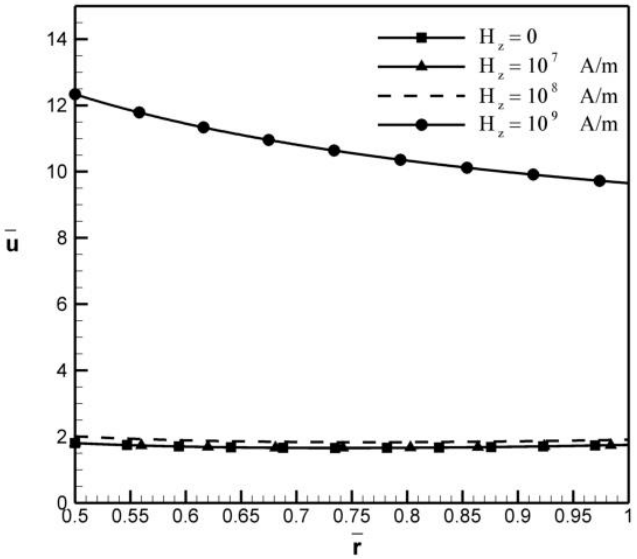

Fig. 15 The effects of magnetic field H_z on the dimensionless radial displacement distribution, ($T_i = 25^{\circ}C$, $T_o = 100^{\circ}C, \beta = 1.2$)

non-homogeneity parameter within a radius of more than 0.75. Fig. 14 demonstrates an increase in non-homogeneity parameter causes an increment in the equivalent strain, the maximum and minimum of which occur on the inner and outer surfaces of the cylinder, respectively.

Figs. 15-17 indicate the displacement field and equivalent stress and strain as a radial function, to which magnetic field effects have been applied. In Fig. 15, increasing magnetic field is shown to enhance radial displacement. Magnetic field of $H_z = 10^9 (^{A}/_{m})$ produces much greater radial

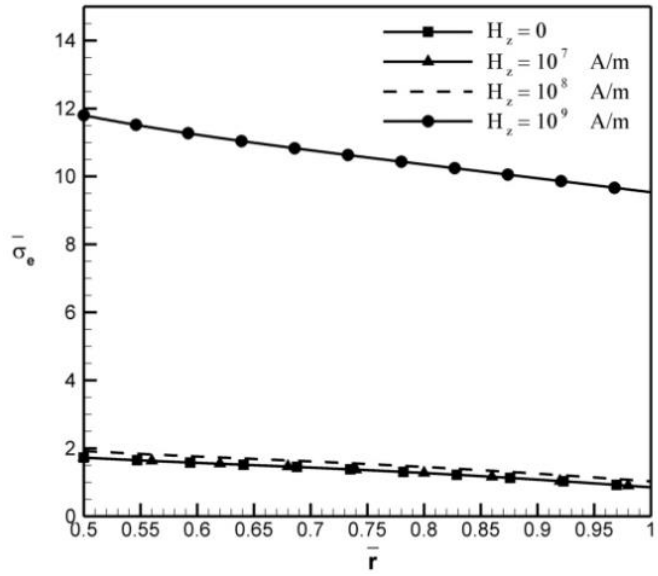

Fig. 16 The effects of magnetic field H_z on the dimensionless equivalent stress distribution, ($T_i = 25^{\circ}C$, $T_o = 100^{\circ}C, \beta = 1.2$)

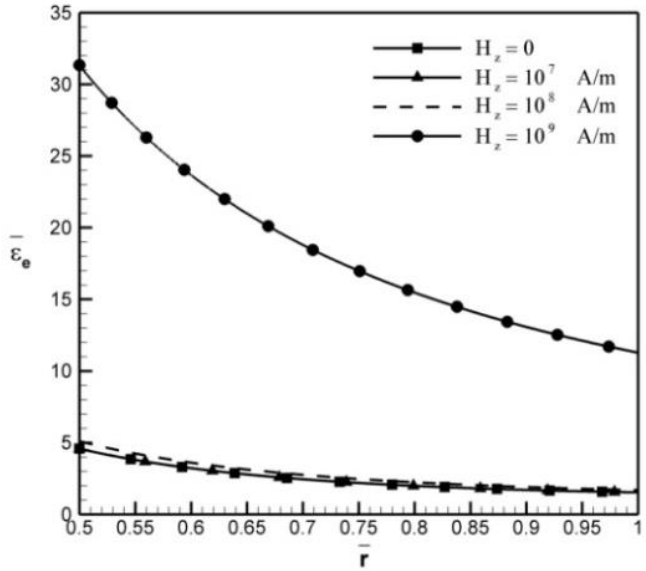

Fig. 17 The effects of magnetic field H_z on the dimensionless equivalent strain distribution, ($T_i = 25^{\circ}C$, $T_o = 100^{\circ}C, \beta = 1.2$)

displacement compared to those induced by other values.

As displayed in Figs. 16 and 17, with increasing magnetic field, equivalent stress and strain values increase. By comparing Figs. 8-10 and Figs. 15-17 based on magneto-elastic solutions, it can be discovered that thermal loading has significant effects on the displacement, stress, and strain fields in such a way that it causes their enhancements within identical magnetic fields.

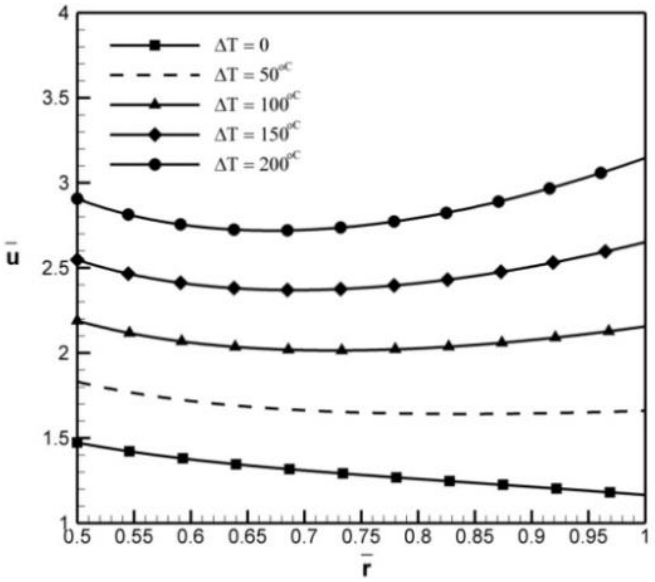

Fig. 18 The effects of temperature difference ΔT on the dimensionless radial displacement distribution. ($T_i = 25^{\circ}C$, $\beta = 1.2$, $H_z = 10^8 (^{A}/_{m})$)

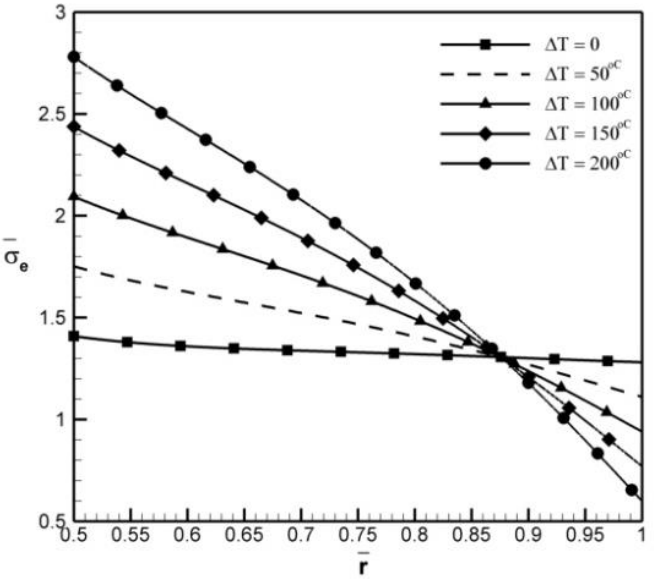

Fig. 19 The effects of temperature difference ΔT on the dimensionless equivalent stress distribution. ($T_i = 25^{\circ}C$, $\beta = 1.2$, $H_z = 10^8 (^{A}/_{m})$)

Also, by comparing magneto-elastic and magneto-thermo-elastic solution, it can be concluded that in the absence of thermal filed, displacement, equivalent stress and strain are reduced by increasing magnetic field strength. It means that applying magnetic field has suitable effects on the elastic response and improves them. Nevertheless, when thermal and magnetic fields are simultaneously imposed, behavior of the cylinder is reversed. It means that due to the presence of

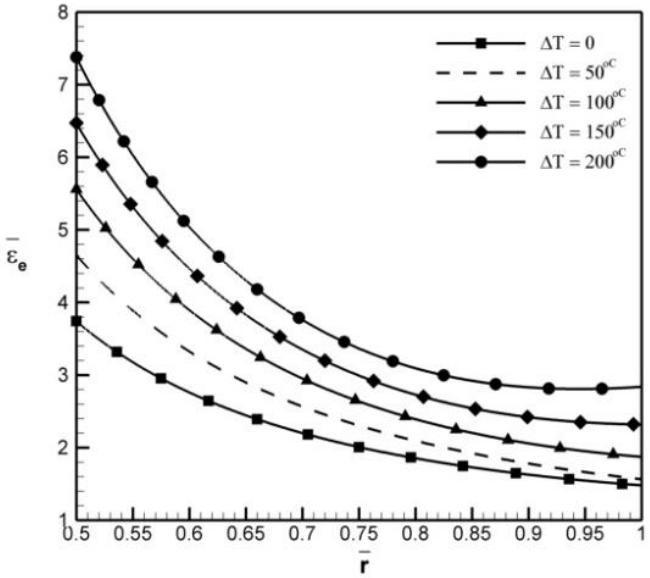

Fig. 20 The effects of temperature difference ΔT on the dimensionless equivalent strain distribution. ($T_i = 25^{\circ}C$, $\beta = 1.2$, $H_z = 10^8 (^A/_m)$)

thermal field, increasing the magnetic field strength results in increasing values of displacement, equivalent stress and strain. Therefore, it should be pointed out that magnetic field has unsuitable effects on the elastic behavior of the FGM hollow cylinder in the presence of a thermal field.

Figs. 18-20 illustrate displacement and equivalent stress and strain distributions in terms of a dimensionless radius at the presence of a magnetic field, to which thermal field effects have been applied. Note that in Figs. 18-20, $\Delta T = T_o - T_i$. According to Fig. 18, it can be observed that radial displacement increases with increasing temperature.

Furthermore, in Fig. 19, it can be seen that the equivalent stress enhances with a temperature rise, while near a radius of 0.87, its behavior changes to decay with increasing temperature. Also, with each temperature amount, the equivalent stress displays a descending behavior in the radial direction. In Fig. 20, it is shown that the equivalent strain values increase with increasing temperature. In the relevant diagram, the minimum and maximum equivalent strains occur on the outer and inner surfaces of the cylinder, respectively.

4. Conclusions

In this paper, the exact solution of stress and strain fields were presented for the cylinders made of FGMs within an external magnetic and temperature fields. It was found that by these materials, the non-homogeneity parameter of β, magnetic field, and temperature distribution have significant effects on the distributions of displacement and equivalent stress and strain. It was further observed that with the values of $H_z \leq 10^7 (^A/_m)$, magnetic field effects are negligible either in the presence or in the absence of a thermal field. Moreover, it can be noted that a magnetic field of $H_z = 10^9 (^A/_m)$ leaves considerable effects on displacement and equivalent stress and strain

distributions. Thermal fields always cause increased levels of equivalent stress and strain and displacement. As shown in the diagrams, it is perceived that magnetic field have suitable effects on stress, strain, and displacement distributions in the absence of temperature in a way that increasing magnetic field leads to decreased amounts of equivalent stress and strain and displacement. However, application of a magnetic field in the presence of a thermal field imposes adverse effects, causing enhanced levels of stress, strain, and displacement.

References

Chattopadhyay, S. (2004), *Pressure Vessels: Design and Practice*, CRC Press, Boca Raton, FL.

Dai, H.L., Fu, Y.M. and Dong, Z.M. (2006), "Exact solutions for functionally graded pressure vessels in a uniform magnetic field", *Int. J. Solid. Struct*., **43**(18-19), 5570-5580.

Dai, H.L. and Wang, X. (2004), "Dynamic responses of piezoelectric hollow cylinders in an axial magnetic field", *Int. J. Solid. Struct*., **41**(18-19), 5231-5246.

Eslami, M.R., Babaei, M.H. and Poultangari (2005), "Thermal and mechanical stresses in a functionally graded thick sphere", *Int. J. Press. Ves. Pip*., **82**(7), 522-527.

Jabbari, M., Sohrabpour, S. and Eslami, M.R. (2002), "Mechanical and thermal stresses in a functionally graded hollow cylinder due to radially symmetric loads", *Int. J. Press. Ves. Pip*., **79**(7), 493-497.

Kraus, J.D. (1984), *Electromagnetic*, McGraw-Hill Inc., New York, USA.

Lutz, M. P. and Zimmerman, R.W. (1996), "Thermal stresses and effective thermal expansion coefficient of a functionally gradient sphere", *J. Therm. Stress*., **19**(1), 39-54.

Naghdabadi, R. and Hosseini Kordkheili, S.A. (2005), "A finite element formulation for analysis of functionally graded plates and shells", *Arch. Appl. Mech*., **74**(5-6), 375-386.

Obata, Y. and Noda, N. (1994), "Steady thermal stresses in a hollow circular cylinder and a hollow sphere of a functionally gradient material", *J. Therm. Stress*., **17**(3), 471-487.

Peng, X. L. and Li, X.F. (2010), "Thermoelastic analysis of a cylindrical vessel of functionally graded materials", *Int. J. Press. Ves. Pip*., **87**(5), 203-210.

Reddy, J.N. and Chin, C.D. (1998), "Thermomechanical analysis of functionally graded cylinders and plates", *J. Therm. Stress*., **21**(6), 593-626.

Ruhi, M., Angoshtari, A. and Naghdabadi, R. (2005), "Thermoelastic analysis of thick-walled finite-length cylinders of functionally graded materials", *J. Therm. Stress*., **28**(4), 391-408.

Tokovyy, Y.V. and Ma, C.C. (2007), "Analysis of 2D non-axisymmetric elasticity and thermoelasticity problems for radially inhomogeneous hollow cylinders", *J. Eng. Math*., **61**(2-4), 171-184.

Tutuncu, N. and Ozturk, M. (2001), "Exact solutions for stresses in functionally graded pressure vessels", *Compos*., **32**(8), 683-686.

Ghannad, M., ZamaniNejad, M., Rahimi, G.H. and Sabouri, H. (2012), "Elastic analysis of pressurized thick truncated conical shells made of functionally graded materials", *Struct. Eng. Mech*., **43**(1), 105-126

Ghannad, M. and Gharooni, H. (2014), "Displacements and stresses in pressurized thick FGM cylinders with exponentially varying properties based on FSDT", *Struct. Eng. Mech*., **51**(6), 939-953.

Saadatfar, M. and Aghaie-Khafri, M. (2015), "Electromagnetothermoelastic behavior of a rotating imperfect hybrid functionally graded hollow cylinder", *Smart. Struct. Syst*., **15**(6), 1411-1437.